Polyaniline film-based wireless photo reactor for hydrogen generation through exciton mediated proton reduction

Smita Masid Roy [a, *], Nageswara N. Rao [a], Alexandre Herissan [b], Christophe Colbeau-Justin [b]

[a] Wastewater Technology Division, CSIR-National Environmental Engineering Research Institute, Nehru Marg, Nagpur 440020 India
[b] Laboratoire de Chimie Physique, CNRS UMR 8000, Université Paris-Sud, Bâtiment 349, Orsay Cedex F-91405, France

ARTICLE INFO

ABSTRACT

The unique light absorption property of semiconductors has been exploited to build photovoltaic (PV), photo electrochemical solar cells (PESC) and photocatalytic (PC) reactors that not only convert sunlight into electrical energy but also drive useful chemical reactions. Hydrogen, the clean fuel of 21st century has been targeted for several decades. However, the above systems possess complex architecture with two or more semiconductor-solution interfaces that are often plagued with material instability and show poor photon conversion efficiency. Here we demonstrate a simple pristine polyaniline (PANI) film based photo H_2 generating system. The 'wireless' system with only one PANI/solution interface, utilizes internal redox chemistry in the conjugated polymer for 'photo exciton' formation and charge separation. The electrons migrate to the PANI/aq. H_2SO_4 interface and reduce H^+ to produce H_2. The polymer film is light weight, flexible, and solution-processable. The reported system is simple and scalable for high volume production of hydrogen.

1. Introduction

Production of new fuels having negligible environment-footprint with the use of renewable energy sources such as sunlight is very attractive. Hydrogen is a clean fuel with little environmental impact. It can be produced through many methods, viz., steam reforming of natural gas [1,2] and ethanol [3], electrolysis of water [4], thermo catalytic reformation of hydrogen-rich organic compounds [5], thermo-chemical splitting [6], and biological processes [7]. Some of these methods depend on electrical energy and feedstock availability which contribute to higher pricing of hydrogen gas. In contrast, hydrogen production using abundant solar energy can work out to be more economical.

The methods that use sunlight viz., PV, PEC and PC reactors have emerged for generating electricity and clean fuels [8—10], and light energy conversion principles using semiconductor (SC)/electrolyte interfaces have been widely investigated [11]. For the photo splitting of water at the semiconductor surface, the conduction band (CB) and valence band (VB) edges (E_{CB} and E_{VB} respectively) must bracket the two redox levels corresponding to the hydrogen evolution reaction (HER) and the oxygen evolution reaction (OER), respectively [11—13]. It is also possible to add sacrificial agents to the solution such that the HER and OER steps may be separately performed [11]. This approach would avoid photo splitting of water, yet generate either H_2 or O_2. For example, the E_{CB} level should be more negative than the HER ($E_{H2/H2O}$) to initiate hydrogen production. Holes (h^+) oxidize a sacrificial electron donor simultaneously. The electrons may be driven into external circuit connected to a metal cathode (Pt) at which H^+ can be reduced to H_2 gas. This concept was verified by many authors [14,15]. We demonstrated simultaneous H_2 generation and pollutant removal in a PEC reactor in which photo-anode (Ti/TiO_2) and Pt cathode were connected externally [15]. However, the rate of HER was low. There must have been considerable loss of electrons during transport through external circuit. To achieve high photocatalytic efficiency for H_2 generation, researchers have also developed methods for compositing semiconductor (SC)-semiconductor, metal/SC, or SC/polymer interfaces etc., accompanied by sacrificial aqueous solution in order to sustain the reaction cycle [16—19].

To overcome this, we conceptualized a 'wireless' PEC reactor comprising of polymer film/SC nanocomposites. According to this, a

* Corresponding author.
E-mail addresses: smitamasid@gmail.com (S.M. Roy), nn_rao@neeri.res.in (N.N. Rao), alexandre.herissan@u-psud.fr (A. Herissan), christophe.colbeau-justin@u-psud.fr (C. Colbeau-Justin).

conducting polymer film, e.g., polyaniline (PANI) can be used with one side of the same holding SC particles while the rear side supports reduction reactions. The side containing SC particles becomes the side of illumination, and the polymer would carry electrons to the rear side of the film. Under suitable conditions a fraction of photo-electrons may be available for reduction reactions on the rear side of the PANI films.

Polyaniline has interesting optoelectronic properties [20]. During our studies with polymer-semiconductor (PANI/CdS) and metal-polymer-semiconductor (Pt/PANI/CdS) nano composite hybrid films, a remarkable ability of pristine PANI films to produce H_2 on the rear side under visible light irradiation of the opposite side was noticed (Supplementary Note S1, Figure S1). We report here the pristine polyaniline film based 'wireless' photo reactor with potential to generate hydrogen gas from aqueous acid solution under sunlight.

2. Experimental details

2.1. Materials

Polyaniline, emeraldine salt having average $M_w > 15,000$ was procured from Alfa Aesar®, USA. N-methyl-2-pyrrolidone (NMP, 99.5%) was purchased from SISCO Research Laboratories Pvt. Ltd. Mumbai, India. The molecular probe, 2′, 7′- dichlorodihydro-fluorescein diacetate (H₂DCFDA) was obtained from Fluka, USA. High purity methanol was used. All the other chemicals, viz, H_2SO_4, NaOH, NH₄OH, phosphate buffer were reagent grade chemicals. Deionized water obtained from Elix 3 Millipore Water Purifier was used for preparing reagents.

2.2. Hand casting of PANI film

Initially, PANI- NMP solution was prepared by dissolving 2 wt% PANI in NMP with continuous stirring for 8–12 h at room temperature. The PANI films were prepared by casting (2%) PANI-NMP solution on a flat glass substrate. Prior to casting, the glass substrate was boiled in 1 M NaOH solution for 15–20 min and dry in hot air oven at 100 °C for 2 h. A fine coat of NaOH was present on the glass surface. The NaOH-coated glass substrate was used for casting thin film of PANI. Approximately 0.5 c. c of PANI-NMP (2%) solution was poured on the glass substrate and spread uniformly with the help of a scalpel. This was dried in hot air oven at 50 °C for 8 h. This was cooled to room temperature and the glass substrate having PANI film was immersed in deionized water for 5 min. A purple/copper colored free standing thin PANI film is peeled off from the glass substrate due to dissolution of underlying NaOH layer. We could not obtain intact PANI films using plain glass substrate; hence, applying a pre coat of NaOH on glass substrate was necessary. Then, the PANI film was washed several times in deionized water for removal of soluble NMP and NaOH. The film was then dried at 50 °C for 8 h. In this way, 30–40 μm thin film of PANI was prepared. It is possible to vary the thickness of PANI film by varying the amount of PANI in casting solution as well as the volume of casting solution.

2.3. Method for removal of NMP

The as-prepared PANI films contain considerable amount of NMP. In this study, NMP- free PANI films were obtained following protonation-deprotonation cycles (PDC) method proposed earlier [21]. Thus NMP-free PANI film obtained after 4 repeated cycles of PDCs. The progress of NMP removal was analyzed by FTIR as well as gravimetric analysis. The as-prepared PANI film showed electrical conductivity, 0.821 S cm⁻¹.

2.4. Analyses

A Fourier-transform infrared absorption spectrophotometer (FT-IR) SPECTRUM GX, (Perkin-Elmer was) used to determine the specific functional groups attributable to PANI. Diffuse Reflectance Spectroscopy (DRS) (Shimadzu UV-3101PC) equipped with an integrating sphere (at room temperature and BaSO₄ reference) was used for determination of band gap energy of PANI in 250–600 nm range. The value E_g for the direct transition in PANI was calculated from reflectance [F(R)] by finding the intercept of the straight line in the low energy rise of a plot of $[F(R_\infty)*h\upsilon]^2$ against the photon energy, (hυ), where, h is plank constant, υ is the frequency of vibration, R is the reflectance, F (R_∞) is Tauc equation which was calculated from the formula, $(1-R)^2/2$ R. The morphology of PANI films was characterized using SEM (Hitachi, S-4800, 18 kV) equipped with an energy dispersive X-ray (EDS) spectrophotometer and operated at 20 kV. CSPM 3000 Atomic Force Microcopy (Primitive) was used for recording AFM images using film size: 0.5 cm² in the scan range: 1 μm × 1 μm. The electrical conductivity of the as-prepared PANI films was determined using Four-Probe Method (DFP-02, SES Instruments Pvt. Ltd, India).

2.5. Gas chromatographic measurements

The H⁺ reduction experiments were performed in a single chamber reactor containing 5.0×10^{-3} N H_2SO_4 (pH ~ 2.03) in contact with internal face of PANI film, while the external face was exposed to sunlight. Pure nitrogen gas was purged through the electrolyte to purge dissolved air Hydrogen evolved during the experiments was analyzed using gas chromatography (Auto System, Perkin Elmer) with TCD, ultra-pure N_2 as carrier gas of flow rate 20 c. c. min.⁻¹, with a packed column of Porapak QS (80/100 mesh, 6' × 1/8" × 0.085″, stainless steel). The GC oven temperature was set at 50 °C and 100 °C for detector. The GC method was calibrated using high purity hydrogen gas standard (99.999%) supplied by Chemtron Science Laboratories Pvt. Ltd. Mumbai. Prior to actual experiments the reactor was tested for leaks by introducing a known volume of hydrogen gas into headspace and checking for constancy in corresponding gas chromatographic peak area as a function of time. Linear regression of the corresponding peak area (y-axis) versus volume (μl, x-axis) plot resulted in equation as $y = 3.7246 \times 10^4$ x with regression coefficient (r^2) equal to 0.99.

2.6. Time resolved microwave conductivity (TRMC) analysis on PANI film surface

The measurement of TRMC was carried out as reported earlier [22]. A Gunn diode in the K_a band (29–31 GHz) was the source of microwaves. The experiments were performed at 30.0 GHz. A Nd:YAG laser pulsed light source provided 1064 nm IR radiation (10 ns Full width at half-maximum; 10 Hz repetition frequency; light energy at the sample surface, 1.3 mJ cm⁻²). IR radiation was tripled to get UV light (355 nm).

2.7. Alkaline hydrolysis of 2′, 7′- dichlorodihydrofluorescein diacetate (H₂DCFDA) on the PANI film surface

The (H₂DCFDA) [23] is oxidized to the fluorescent 2′, 7′-dichlorofluorescein (DCF) in the presence of reactive oxygen species (e.g., hydroxyl radicals). For this purpose, 4.9×10^{-3} g of H₂DCFDA solution was added to 10 ml methanol to prepare 1 mM (H₂DCFDA) solution, 500 μL of this was then added to 2 ml of 0.01 N NaOH and after 30 min, 10 ml 25 mM phosphate buffer at pH 7.4 was then added to the above solution mixture (i.e. H₂DCFDA/methanol/NaOH solution). About 50 μl of prepared solution

mixture was then spread on the prepared PANI film surface and this was observed under Fluorescence microscope (Olympus BX51) at 545 nm (10 × magnification).

3. Results and discussion

3.1. Characterization of PANI film

The prepared hand casting free-standing lustrous PANI film has thickness about 30–40 μm. The different redox states, electrical conductivity and color variations are given in Table 1. Emeraldine base (EB) is slightly less conducting (0.83 ± 0.02 Scm^{-1}) compared to emeraldine salt (ES, 1.05 ± 0.02 Scm^{-1}). Pernigraniline shows very poor conductivity.

PANI displays all the characteristic IR absorptions (Table S1), the main peaks at 1587 cm^{-1} due to C=C stretching mode of the quinoid rings, and another at 1502 cm^{-1} due to C=C stretching mode of benzenoid were observed. The UV–vis DRS spectra for PANI (Figure S2) show an absorption peak at about 320–350 nm, a shoulder at 420 and absorption tail starting from 540 nm and extending up to 800 nm. The absorption peak at 320–350 nm is assigned to π-π^* transition of the conjugated benzenoid rings. The polaron and bipolaron band transitions in polyaniline occurred at 420 and 540–800 nm [24–28]. The band gap of PANI film was estimated to be 2.85 eV. The PANI film is highly granular, irregular in shape and has porous structure (Figure S3). The average grain size was found to be 2–4 μm. The surface of the polyaniline film consists of nodular growth with distinct grain boundaries as seen in AFM images.

3.2. Photo electron transfer across PANI film and H$^+$ reduction in wireless system - H$_2$ evolution

The schematic of the photo-reactor is depicted in Fig. 1. In this single chamber 55 c. c. cylindrical reactor fabricated using Acrylic® pipe and side plates, a PANI film was fixed onto a circular hole (ϕ, 1.60 cm) drilled into one of the side plates. The film was fit by special screw-cap accessory and made leak-proof. The film interfaces with electrolyte in the chamber (internal face, IF) while the external face (EF) was exposed to sunlight. Another side plate can be fixed to the reactor optionally to create two chambers in which the EF can also interface with an electrolyte containing a sacrificial electron donor (SED e.g., K$_4$Fe(CN)$_6$). The reactor has provisions for introducing electrolyte into the chamber and for withdrawing gases from the headspace through a septum. The chamber was filled with electrolyte (0.025 M FeCl$_3$, pH 2) leaving 5 c. c. head space volume. At first, the ability of PANI film to transfer electrons across its thickness was verified by conversion of Fe^{3+} to Fe^{2+} at PANI (IF) according to a reported approach [28] using a two-chamber reactor in which PANI (EF) interfaced with K$_4$Fe(CN)$_6$

electrolyte. The conversion of Fe^{3+} to Fe^{2+} was analyzed by complex formation with 1, 10 phenanthroline by measuring absorption at λ_{max} 510 nm spectrophotometrically. We found that the reduction of Fe^{3+} can proceed even in a single chamber reactor where PANI (IF) only makes interface with ferric chloride solution and PANI (EF) was dry and illuminated with sunlight. The extent of reduction of Fe^{3+} at PANI film (IF) under solar irradiation of external face is depicted in Fig. 2a. The observed rate of Fe^{2+} formation was ~48.38 mM h^{-1}. The reduction of Fe^{3+} was observed repeatedly using fresh PANI films. It is concluded that irradiation of external surface of pristine PANI films leads to reduction of electron acceptors available at the internal face confirming that the PANI film supports transfer of electrons across it.

We predicted that H$^+$ from an acidified solution may be reduced at the internal face of the PANI film and possibly generate H$_2$. The procedure of H$^+$ reduction experiments and GC determination of evolved H$_2$ gas is given elsewhere (Figure S4). Upon irradiation of the external surface of PANI film under solar light, H$^+$ was reduced at PANI (IF) and H$_2$ gas was evolved. A total of 887 ± 20 μmol H$_2$ was produced at a rate of 98.77 μmol h^{-1} in 8 h (Fig. 2b). This was checked repeatedly using fresh PANI films. Control experiments involving i) replacement of aqueous sulfuric acid solution with deionized water, and ii) replacing PANI film with non-conducting polyethylene film, were conducted. In both the cases no H$_2$ was evolved (Fig. 2c). Thus both PANI film and aq. H$_2$SO$_4$ are necessary for H$_2$ evolution.

The rate of H$_2$ evolution may depend on the exposed area of PANI film because larger area implies more photo-electrons and hence more hydrogen evolution. Fig. 2d shows that the rate of H$_2$ evolution indeed increases with increase in the exposed area of PANI films. About 106, 331 and 467μmoles H$_2$ was evolved using PANI films having exposure areas of 0.19645, 0.9506 and 1.54 cm^2, respectively. The corresponding initial rates of H$_2$ evolution were 19.52, 63.00, 87.30 μmol h^{-1}. The rates normalized to exposed area are: 99.46, 66.27 and 56.67 μmol h^{-1}cm^2. This suggests that the rate of hydrogen evolution is not directly proportional to the exposed area of PANI film. This may be due to non-uniformities in the texture and micro scale conductivity of larger PANI films as they are hand cast.

It is important to know whether a used PANI film can be reused for generating H$_2$. We conducted H$^+$ reduction experiments repeatedly for 4 times using the same PANI film while all the other experimental conditions were essentially fixed and comparable. Fig. 2 (e) shows that the hydrogen generating ability of the PANI film in all the 4 runs is comparable. The PANI films show good stability towards H$_2$ evolution and they may be expected to maintain activity over several more reuse cycles.

Thus sunlight irradiation of external surface of PANI films reduces electron acceptors available at the internal face. This may be rationalized as follows. Polyaniline properties are dependent on its

Table 1
Different polyaniline states, electrical conductivity (EC), and their observed color variations.

Attribute	Polyaniline States		
	Emeraldine base (EB)	Emeraldine salt (ES)	Pernigraniline
EC (S cm^{-1})	0.8287 ± 0.02 (4.1435 ± 0.02)[a]	1.0456 ± 0.02 (6.2736 ± 0.02)[a]	0.000231 ± 0.02
Color Image/color	Copper-Brown	Dark green	Deep Violet

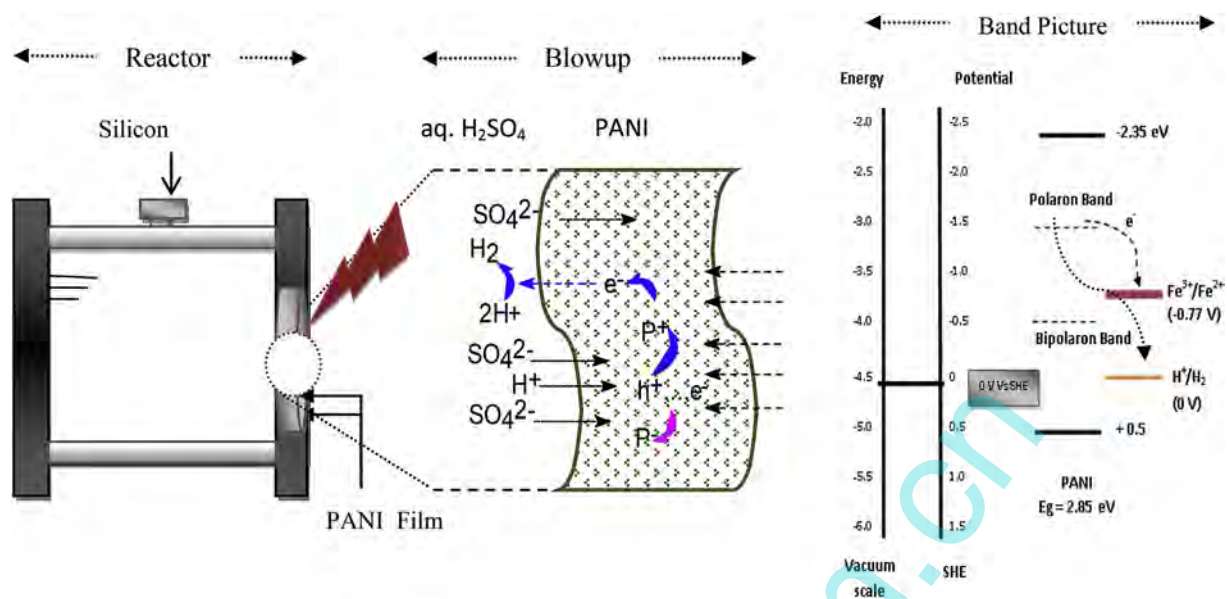[a] Under irradiation [tungsten bulb, 100 W].

Fig. 1. (Reactor) Schematic of photo reactor using PANI film for hydrogen evolution under sunlight; (blowup) shows tentative events in the illuminated PANI film depicting polaron generation, migration of charges to the internal face, and proton reduction; (band picture) photo excitation and pathway for e^- transfer at PANI film involving 'polaron' and 'bipolaron' levels' which have more negative potential than E^0_{red} (Fe^{3+}/Fe^{2+}, -0.77 V vs SHE) and E^0_{red} (H^+/H_2), 0.0 V vs SHE). (For interpretation of the references to colour in this figure legend, the reader is referred to the web version of this article.)
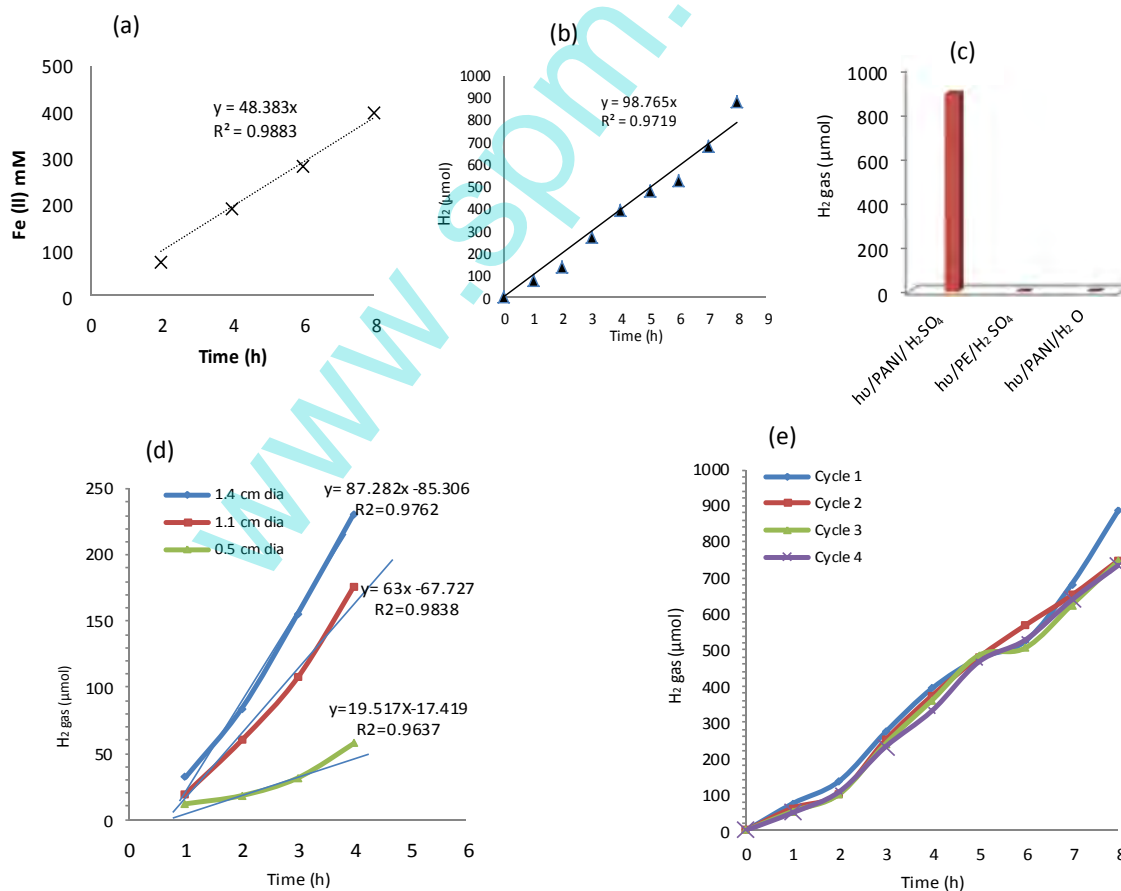

Fig. 2. (a) Fe (III) to Fe (II) reduction in solar PEC reactor with PANI film in the absence of sacrificial electron donor and (b) H^+ reduction and H_2 generation with solar irradiated PANI film in single compartment PEC reactor, and (c) control experiments to assess the suitable conditions for H^+ reduction in the absence of sacrificial electron donor, (d) Dependence of solar hydrogen gas generation on the exposed area of the PANI film and (e) reusability of PANI film for solar H_2 generation.

oxidation and protonation state. Acid treatment results in more conducting emeraldine salt (ES) and de-doping in base solution yields emeraldine base state (EB) [29]. In the present study, the NMP free films appear to still contain some Cl^- as dopant as can be understood from the observed conductivity, 0.83 Scm^{-1}. When the film interfaces with aq. H_2SO_4, chemical doping takes place, both protons and sulfate anions are incorporated into the polymer matrix. Such dopant exchange behavior in PANI films has been previously reported, and SO_4^{2-} doped films registered a moderate increase in conductivity compared to the Cl^- - doped PANI films [30], as also observed in this study. The PANI emeraldine salt transforms into positive polarons (P^+) through internal redox reaction (see Scheme I, proton doping). On the other hand, when the PANI film is irradiated with sunlight electrons (e^-) - hole (h^+) pairs are created. This results in the oxidation of a part of the polymer chain into positive polarons (P^+), while the other part gets reduced by electrons forming a radical anions (P^-), called negative polarons (see Scheme I, photo doping). The electrons are promoted across the band gap when the polymer film is exposed to radiation of sufficient energy during photo doping process [31–34]. The polaron is localized partly due to coulomb attraction to counter ions and partly due to local changes in its equilibrium geometry relative to the neutral molecule [35]. This represents a destabilized bonding orbital and hence has higher energy than that of valence band. In this study, polaron formation is inferred from the absorption shoulder at 420–450 nm in UV−vis DRS spectra [11–14] as well as strong paramagnetic response from the isolated electrons (Figure S5). Single electron bearing isolated polaronic states are typically paramagnetic [36]. The polarons may combine to give rise to bication (2 P^+) radicals, bianion (2P^-) radicals, and neutral bipolarons (2 P^0) [37]. They can be treated as localized new electronic states within the band gap. In the present study, the formation of bipolarons can be inferred from gradually increasing

absorption tail in UV-DRS spectrum in the 500–800 nm. Such absorption tail was earlier interpreted as due to bipolaron formation [25].

Several such polaronic states within the band gap may overlap especially when the dopant concentration is high, creating a band of energy levels corresponding to polarons and bipolarons. As per the energy band picture (Fig. 1), the polaron band is located at relatively more negative potential compared to the E_{red} (Fe^{3+}/Fe^{2+}) which is −0.77 V vs SHE and the electrons are transferred to Fe^{3+} causing reduction into Fe^{2+}. Similarly, since the polaron and bipolaron bands are located at relatively more negative potential compared to the E_{red} (H^+/H_2), which is 0.0 V vs SHE, the electrons readily reduce H^+ causing H_2 evolution (Fig. 1). In this study, PANI film was exposed to intense sunlight ~1370 W/m^2. We observed a 4–6 times increase in electrical conductivity due to photo-irradiation of PANI films which may be due to increase in the number of charge carriers due to photo-doping (Table 1). This is another reason for the enhancement in the photo-activity of PANI film (Fig. 2c).

The observed photo response of PANI films can be linked to excess charge-carrier dynamics. To understand charge-carrier dynamics we performed TRMC measurements on the PANI film samples. TRMC measurements have been frequently used to correlate photo activity of semiconductors with charge carrier dynamics [22]. Fig. 3(a and b) shows the TRMC signals obtained by laser irradiation of PANI films at 355 and 532 nm, respectively.

The TRMC signal can be attributed to electrons. The mobility of electrons is greater than that of holes. Two observations are important: (i) the I_{max}, which reflects the number of excess charge-carriers is approximately 3 times greater at 532 nm compared to that at 355 nm; and (ii) a limiting I_{max} value was attained in both the cases and the excess charge-carriers did not decay within the time scale, < 0.10 μs, they are relatively long-lived excitons. The
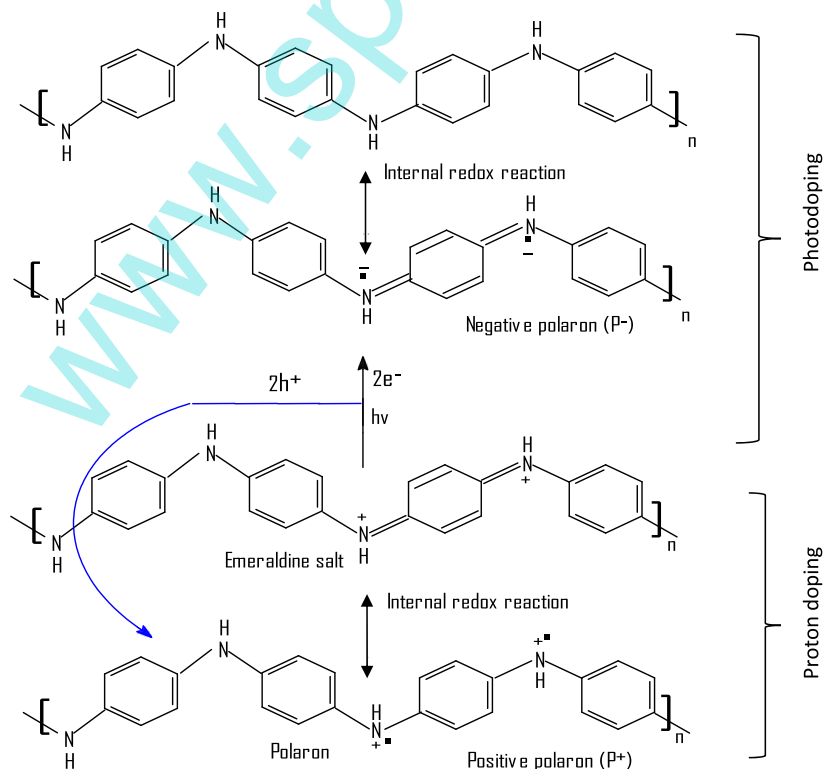
Scheme I. (Proton doping) Acid base equilibrium showing inter conversion of PANI emeraldine base into salt and vice versa, internal redox reaction leading to polaron formation; (Photo doping) hole-mediated oxidation of PANI (ES) to positive polaron (P^+) and electron-mediated reduction of PANI (ES) to Negative polaron (P^-).

greater I_{max}, at 532 nm implies that PANI films generate more number of charge carriers under visible light; while the limiting I_{max} values mean that the rate of decay of excess electrons is insignificant due to very large relaxation time of trapped holes. It is inferred from the TRMC data that stabilization of polaronic states in the PANI film occurs and excess charge-carriers (trapped electrons or equivalent radicals) may be available for surface reactions under suitable conditions. These charge-carriers at the film surface can react with adsorbed oxygen on the surface of a PANI film and reactive oxygen species (ROS) such as singlet oxygen, super oxides, peroxides, and OH radicals may form. To confirm this, we used a molecular probe 2′, 7'-dichlorodihydrofluorescein diacetate (H_2DCFDA) that gets oxidized to the fluorescent 2′, 7'-dichlorofluorescein (DCF) by ROS on the surface of a PANI film. This technique is frequently employed to detect ROS bound to particles and surfaces [23]. The experimental procedure has mentioned in section 2.7. The corresponding fluorescence microscopy images depicting the surfaces of neat PANI film ('a'), the film surface on which probe molecules were introduced ('b') and acid quenching of fluorescence ('c') are shown in Fig. 4. The neat PANI film showed no fluorescence. Fig. 4b clearly shows structured regions on the surface due to formation of fluorescent 2′,7'- dichlorofluorescein (DCF). The fluorescent regions appear to represent zig-zag polymeric strands may be representing trapped charges along the grain boundaries. The trapped electrons reduce surface oxygen into ROS. The ROS in turn oxidize H_2DCFDA into fluorescing DCF molecules. The observed fluorescence from DCF was quickly quenched by adding dilute H_2SO_4 as shown in the image 'c'. It was also verified that PANI surface which was previously immersed in H_2SO_4 does not give rise to fluorescence. This suggests that H_2SO_4 is probably a competitor for H_2DCFDA, and trapped electrons are shunted to reduce H^+ into H_2. Defects and grain boundaries may also act as hole traps [38,39]. The observed continuous generation of hydrogen can be linked to effective charge transport of electrons across the PANI film, involving intra- and inter-chain charge migration processes. This may become possible due to continued
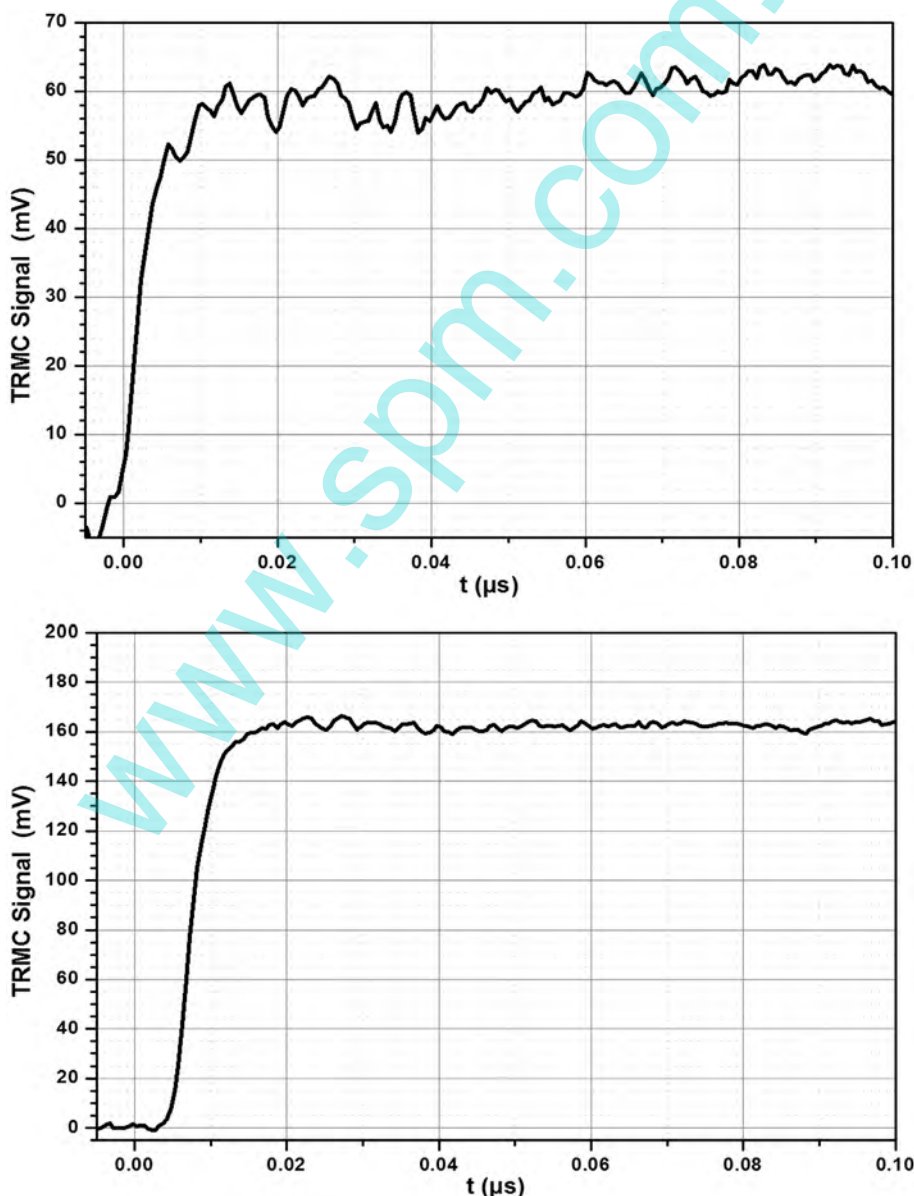

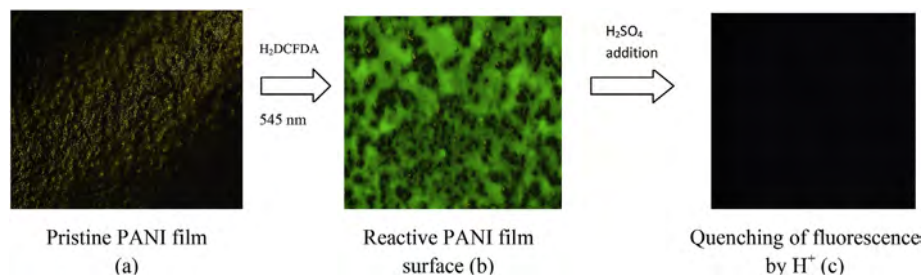**Fig. 3.** TRMC response of PANI film at 355 (a) and 532 nm (b).

Fig. 4. Fluorescence microscopy images depicting (a) surface of pristine PANI film, (b) the film surface on which probe molecules were introduced and (c) quenching of fluorescence by H_2SO_4.

contact of inner face of PANI film with sulfuric acid, the SO_4^{2-} concentration in the polymer may become high which surround and stabilize polarons [40,41]. A part of photo electrons may also recombine with trapped holes and generate neutral polymer subunits.

Thus, the results discussed above confirm that H_2 is generated at PANI/H_2SO_4(aq.) using the excitons generated within PANI film. Though the exact mechanism is arguable at this stage, our results confirm the functional use of PANI films for hydrogen production. There are a few research articles that deal with exciton mediated reactions. For example, exciton mediated chemical reactions (e.g., silylation) on the surface of semiconductors have been previously reported [42]. Recently, a metal-free polymeric carbon nitride photocatalyst powder was shown to produce hydrogen from water containing triethanolamine as a sacrificial electron donor under visible light and continuous H_2 evolution amounting to 770 μmol in 72 h was reported [43]. A molecular molybdenum-oxo catalyst for electrochemical hydrogen production (2.4 mol of H_2 per mole of catalyst per second) from neutral buffered water has also been reported [44], but it needs application of bias potential. In a related context, a wireless solar water splitting system using silicon-based semiconductors was reported [45], but the system is very complex comprising a cobalt oxygen evolving catalyst (Co-OEC), a nickel-molybdenum-zinc hydrogen evolving catalyst (NiMoZn), and a triple junction amorphous silicon (3jn-a-Si) interface between the catalysts which is coated with indium tin oxide.

4. Conclusion

In summary, we demonstrated a simple pristine PANI film based photo H_2 generating system. Hydrogen is produced by the reduction of H^+ at PANI/aq. H_2SO_4 interface using excess charge-carriers generated through visible light irradiation of external surface of PANI film. Our system is much simple with the active component (PANI) having only one wet interface, i.e. hν/PANI/aq. H_2SO_4. The present H_2 producing system has no parallels in the known hydrogen generation techniques. The wireless device which can be deployed for H_2 production needs no exotic fabrication and engineering skills and approaches as simple as spreading free-standing PANI film over acidified water can also be explored. Any future wireless device which may be developed based on the present results may emerge as low-cost H_2 producing system. The present work may also inspire further research towards understanding optical properties of PANI in more detail, and conducting polymers in general.

Acknowledgements

respectively. This MS has KRC No.: CSIR-NEERI/KRC/2017/Jan/WWTD/1.

Appendix A. Supplementary data

Supplementary data related to this article can be found at http://dx.doi.org/10.1016/j.polymer.2017.02.013.

References

[1] B. Mustafa, Potential importance of hydrogen as a future solution to environmental and transportation problems, Int. J. Hydrogen Energy 33 (2008) 4013–4029.

[2] A. Haryanto, S. Fernando, N. Murali, S. Adhikari, Current status of hydrogen production techniques by steam reforming of ethanol: a review, Energy fuels. 19 (2005) 2098–2106.

[3] J.D. Holladay, J. Hu, D.L. King, Y. Wang, An overview of hydrogen production technologies, Catal. Today 139 (2009) 244–260.

[4] L.G. Bloor, P.I. Molina, M.D. Symes, L. Cronin, Low pH electrolytic water splitting using earth-abundant metastable catalysts that self-assemble in situ, J. Am. Chem. Soc. 136 (2014) 3304–3311.

[5] H.F. Abbas, W.M.A. Wan Daud, Hydrogen production by methane decomposition: a review, Int. J. Hydrogen Energy 35 (2010) 1160–1190.

[6] K. Onuki, S. Kubo, A. Terada, N. Sakaba, R. Hino, Thermochemical water-splitting cycle using iodine and sulfur, Energy Environ. Sci. 2 (2009) 491–497.

[7] I. Yacoby, et al., Photosynthetic electron partitioning between [FeFe]-hydrogenase and ferredoxin:NADP -oxidoreductase (FNR) enzymes in vitro, Proc. Natl. Acad. Sci. U. S. A. 108 (2011) 9396–9401.

[8] M. Gratzel, Photovoltaic and photoelectrochemical conversion of solar energy, Philos. Trans. R. Soc. Lond. Ser. A 365 (2007) 993–1005.

[9] R.E. Blankenship, et al., Comparing photosynthetic and photovoltaic efficiencies and recognizing the potential for improvement, Science 332 (2011) 805–809.

[10] M. Walter, et al., Solar water splitting cells, Chem. Rev. 110 (2010) 6446–6473.

[11] K. Rajeshwar, Fundamentals of semiconductor electrochemistry and photo-electrochemistry, in: Encyclopedia of Electrochemistry, Wiley-VCH Verlag GmbH & Co. KGaA, Weinheim, Germany, 2007.

[12] K. Hashimoto, H. Irie, A. Fujishima, TiO_2 Photocatalysis: a historical overview and future prospects, AAPPS Bull. 17 (2007) 12–28.

[13] A. Kudo, Y. Miseki, Heterogeneous photocatalyst materials for water splitting, Chem. Soc. Rev. 38 (2009) 253–278.

[14] T. Bak, J. Nowotny, M. Rekas, C.C. Sorrell, Photo-electrochemical hydrogen generation from water using solar energy. Materials-related aspects, Int. J. Hydrogen Energy 27 (2002) 991–1022.

[15] N.N. Rao, S. Dube, Photoelectrochemical generation of hydrogen using organic pollutants in water as a sacrificial electron donors, Int. J. Hydrogen Energy 21 (1996) 95–98.

[16] M.-H. Hsu, C.-J. Chang, H.-T. Weng, Efficient H2 production using Ag2S-Coupled ZnO@ZnS Core−Shell nanorods decorated metal wire mesh as an immobilized hierarchical photocatalyst, ACS Sustain. Chem. Eng. 4 (2016) 1381–1391.

[17] C.-J. Chang, K.-W. Chu, ZnS/polyaniline composites with improved dispersing stability and high photocatalytic hydrogen production activity, Int. J. Hydrogen Energy 41 (2016) 21764–21773.

[18] C.-J. Chang, K.-W. Chu, M.-H. Hsu, C.-Y. Chen, Ni-doped ZnS decorated graphene composites with enhanced photocatalytic hydrogen-production performance, Int. J. Hydrogen Energy 40 (2015) 14498–14506.

[19] C.-J. Chang, Z. Lee, M. Wei, C.-C. Chang, K.-W. Chu, Photocatalytic hydrogen production by magnetically separable Fe3O4@ZnS and NiCo2O4@ZnS coreeshell nanoparticles, Int. J. Hydrogen Energy 40 (2015) 11436–11443.

[20] E.T. Kang, K.G. Neoh, K.L. Tan, Polyaniline: a polymer with many interesting intrinsic redox states, Prog. Polym. Sci. 23 (1998) 277–324.

[21] E.A. Ponzio, R. Echevarria, G.M. Morales, C. Barbero, Removal of N-methyl-pyrrolidone hydrogen bonded to polyaniline free-standing films by protonation-deprotonation cycles or thermal heating, Polym. Int. 50 (2001) 1180–1185.

[22] C. Colbeau-Justine, M. Kunst, Structural influence on charge-carrier lifetimes in TiO$_2$ powders studied by microwave absorption, J. Mater. Sci. 38 (2003) 2429–2437.

[23] C.A. Cohn, S.R. Simon, M.A. Schoonen, Comparison of Fluorescence-based techniques for the quantification of particle-induced hydroxyl radicals, Part. Fibre Toxicol. 5 (2008) 1–9.

[24] W. Yin, E. Ruckenstein, Soluble polyaniline co-doped with dodecyl benzene sulfonic acid and hydrochloric acid, Synth. Met. 108 (2000) 39–46.

[25] N. Kuramoto, A. Tomita, Aqueous polyaniline suspensions: chemical oxidative polymerization of dodecylbenzene-sulfonic acid aniline salt, Polymer 38 (1997) 3055–3058.

[26] Y. Sun, A.G. MacDiarmid, A.J. Epstein, Polyaniline: synthesis and characterization of pernigraniline base, J. Chem. Soc. Chem. Commun. (1990) 529–531.

[27] B.C. Roy, M.D. Gupta, L. Bhoumik, J.K. Ray, Spectroscopic investigation of water-soluble polyaniline copolymers, Synth. Met. 130 (2002) 27–33.

[28] M. Matsumra, T. Ohno, S. Saito, M. Ochi, Photocatalytic electron and proton pumping across conducting polymer films loaded with semiconductor particles, Chem. Mater 8 (1996) 1370–1374.

[29] M.M. Ayad, A.F. Rehab, I.S. El-Hallag, W.A. Amer, Investigation of the dopant exchange behavior of polyaniline hydrochloride films upon addition of sulfuric acid, Int. J. Polym. Anal. Charact. 14 (2009) 389–402.

[30] W.W. Focke, G.E. Wnek, Conduction mechanisms in polyaniline (emeraldine salt), J. Electroanal. Chem. 256 (1988) 343–352.

[31] S. Stafstorm, et al., Polaron lattice in highly conducting polyaniline: theoretical and optical studies, Phys. Rev. Lett. 59 (1987) 1464–1467.

[32] A.G. MacDiarmid, "Synthetic metals": a novel role for organic polymers (nobel lecture), Angew. Chem. Int. Ed. 40 (2001) 2581–2590.

[33] P. Kar, Doping in Conjugated Polymers, John Wiley & Sons, 2013.

[34] N.D. Sankir, M. Sankir, M. Parlak, Electrical properties and photoconductivity of polyaniline/sulfonated poly (arylene ether sulfone) composite films, Appl. Phys. A 95 (2009) 589–594.

[35] S. Elmas, W. Beelders, J. Nash, T.J. Macdonald, M. Jasieniak, H.J. Griessera, T. Nann, Photo-doping of plasma-deposited polyaniline (PAni), RSC Adv. 6 (2016) 70691–70699.

[36] J. Niklas, et al., Highly-efficient charge separation and polaron delocalization in polymer-fullerene bulk-heterojunctions: a comparative multi-frequency EPR and DFT study, Phys. Chem. Chem. Phys. 15 (2013) 9562–9574.

[37] A.J. Heeger, Semiconducting polymers: the third generation, Chem. Soc. Rev. 39 (2010) 2354–2371.

[38] A. Kohler, Organic semiconductors: No more breaks for electrons, Nat. Mater 11 (2012) 836–837.

[39] J.C. Bolinger, L. Fradkin, K.-J. Lee, R.E. Palacios, P.F. Barbara, Light-assisted deep-trapping of holes in conjugated polymers, Proc. Natl. Acad. Sci. U. S. A. 106 (2009) 1342–1346.

[40] M.M. Kerileng, et al., Electronics of conjugated polymers (I): polyaniline, Int. J. Electrochem. Sci. 7 (2012) 11859–11875.

[41] M. Reghu, Y. Cao, D. Moses, A.J. Heeger, Counterion-induced processibility of polyaniline: transport at the metal-insulator boundary, Phys. Rev. B 47 (1993) 1758–1764.

[42] M.P. Stewart, J.M. Buriak, Exciton-mediated hydrosilylation on photoluminescent nanocrystalline silicon, J. Am. Chem. Soc. 123 (2001) 7821–7830.

[43] W. Xinchen, et al., A metal-free polymeric photocatalyst for hydrogen production from water under visible light, Nat. Mater. 8 (2009) 76–80.

[44] H.I. Karunadasa, C.J. Chang, J.R. Long, A molecular molybdenum-oxo catalyst for generating hydrogen from water, Nature 464 (2010) 1329–1333.

[45] Y.R. Steven, et al., Wireless solar water splitting using silicon-based semiconductors and earth-abundant catalysts, Science 334 (2011) 645–648.